

Response of Indian East coast upwelling to river runoff in an OGCM

C. P. Neema and P. N. Vinayachandran

Centre for Atmospheric and Oceanic Sciences and Divecha Centre for Climate Change

Indian Institute of Science, Bengaluru, India

June 19, 2023

Abstract

Along the east coast of India (ECI), local winds are oriented alongshore during the summer monsoon, favouring coastal upwelling. The East India Coastal Current (EICC) during this period converges at 17°N with northward flow from the south and southward flow from the north. A high-resolution Ocean general circulation model (OGCM) which includes runoff from major rivers (RIVER) simulates the upwelling along the east coast of India during the summer monsoon reasonably well. The model simulation shows that the upwelling increases towards south, where salinity influence is lesser compared to northern parts. The presence of rivers suppresses upwelling, the depth of the source of subsurface water becomes shallow from 100 to 60 m, and reduces the SST cooling by 0.5°C owing to the increase in stratification of the water column.

Key words: ECI, upwelling, Stratification, cooling, RIVER and NORIVER experiments.

1 Introduction

Coastal upwelling is a natural oceanographic process that involves the movement of subsurface cold nutrient-rich water to the surface altering the biological productivity of the region. It occurs as a result of the ocean's surface water being pushed away from the coast by the wind, to be replaced by water from beneath. Coastal upwelling occurs when winds blow parallel to the coast. Supply of nutrients and minerals from the subsurface ocean to the upper layers fuels the growth of phytoplankton, supports the food chain, and promotes fisheries. Most of the major upwelling systems are located along the eastern boundaries of the ocean; examples are California, Peru-Chile, Portugal-Northwest Africa, and Southwest Africa, where the prevailing winds are equatorward [Kämpf and Chapman, 2016]. Seasonal upwelling occurs along Somalia, Sumatra, Yemen, South China Sea, southwest coast of India, southern tip, east coast of India (ECI), and the Sri Lankan dome region [Vinayachandran et al., 2021, Hood et al., 2017] despite the eastern or western orientation of the coast.

Along the ECI, local winds are oriented alongshore and northwards favouring upwelling during the summer monsoon [Shetye et al., 1991, Rao et al., 1995, Thushara and Vinayachandran, 2016]. The winds become favourable for upwelling during the pre-monsoon itself [Rao and Rao, 1989] and upwelling has been reported along Vishakapatnam coast from February which continues till July [Rao et al., 1986]. Upwelling was found to extend spatially offshore till 50 km from 13° to 18°N along the east coast [Rao, 2002]. The barrier layer formed in the BoB caused by the increased stratification due to river influx can inhibit the upwelling in the region [Behara and Vinayachandran, 2016]. Thushara and Vinayachandran [2016] showed that the upwelling was impacted by the river water during the later part of the monsoon season along the ECI. In addition to the freshwater discharge and alongshore wind stress, mesoscale eddies, remote winds from the equator, and wave propagation from the interior of the bay modulate

coastal upwelling in this region [Vinayachandran et al., 2021]. Amol et al. [2020] and Thushara and Vinayachandran [2016] have examined the impact of upwelling on the chlorophyll blooms in the northwestern bay and found that an increase in stratification limits the vertical supply of nutrients in the upwelling regions along the east coast. Thushara and Vinayachandran [2016] cited upwelling and a minor role from advection as the cause for the transport of nutrients from the coast to the offshore in the northern bay. Recently Dey and Sil [2023] noticed active and break phases in upwelling using HF radar data. They observed that, despite the Ekman transport showing upwelling favourable conditions from April to August, SST and currents exhibited upwelling until mid-June and then ceased to exist as a result of two processes; stratification by freshwater and the arrival of a downwelling Kelvin wave. Ray et al. [2022] similarly reported that the upwelling Kelvin wave during January to April triggered coastal upwelling along the northeast coast of India and it was suppressed by a downwelling Kelvin wave during April-August. The propagation of the upwelling and downwelling Kelvin waves weakens along the western boundary of the bay due to the prevailing circulation in this region. The poleward flowing EICC and a clockwise eddy in the head bay seems to play a significant role in this weakening [Rao et al., 2010].

With the advance of the summer monsoon, freshwater discharge into the BoB increases, lowering the salinity in the region. A decrease or increase in rainfall or river discharge can cause significant changes in the surface salinity of the bay. Stratification induced by low salinity water can have important implications on the ECI upwelling as the rivers flow equatorward in this region. A numerical modeling study by Johns et al. [1992], forced with southward transport of water of Hugli and Mahanadi rivers showed the suppression of upwelling north of Vishakapatnam by the low salinity plume and this effect decreased south of it.

Thushara and Vinayachandran [2016] studied the chlorophyll blooms in the western bay during upwelling through model experiments. In particular, they examined the bloom dynamics

associated with stratification induced by river flux and wind transports. As the upwelling process diverts the plume away from the coast, low salinity by river flux had little or no impact on the blooms. There have not been any attempts to quantify the role of rivers in upwelling in this region. In this study, we have used a high-resolution (nearly 13 km) ocean model to simulate the features of upwelling, and the role played by river runoff in modulating the upwelling along the ECI during the summer monsoon using ocean model experiments. We find that the river-induced stratification plays an important role in suppressing upwelling in the northern section of the east coast. The paper is organised as follows. Section 2 provides a brief overview of the model simulations, data, methodology, and validation. In sections 3 and 4, we discuss how the model simulates upwelling in the BoB and the effect of rivers on it. A description of river-induced stratification is provided in Section 5, and a conclusion and summary are given in Section 6.

2 Model, data, and methodology

A global ocean general circulation model (MOM version 5.1) with a horizontal resolution $1/8^\circ$ (approximately 13 km in the Bay of Bengal) has been used for the present study [Vinayachandran et al., 2022]. The model has 42 vertical levels with a resolution of 5 m in the upper 55 m and the resolution decreases exponentially with depth. The horizontal grid is tripolar and the topography is based on Sindhu et al. [2007]. The vertical mixing scheme is KPP [Large et al., 1994] with the bulk Richardson number set to 0.3. For horizontal mixing, a combination of Laplacian and biharmonic friction with a Smagorinsky mixing coefficient of 0.01 and 0.1 respectively, has been used. CORE II [Large and Yeager, 2009] data sets are used for long wave, short wave, air temperature, specific humidity, winds, snow, and rainfall data. Chlorophyll data, used for the parametrization of shortwave penetration in the ocean, is monthly and was

acquired from SeaWiFS.

Rivers entering the ocean are distributed horizontally and vertically by the prevailing current systems in accordance with the thermohaline circulation. In the Indian Ocean, river runoff and its advection lead to large inter-annual variability in salinity near the river mouths and in the eastern equatorial Indian Ocean [Vinayachandran and Nanjundiah, 2009]. Kurian and Vinayachandran [2006] used the spreading method to incorporate river discharge into the modular ocean model; runoff from each river is spread over a horizontal area proportional to its discharge rate over time. In addition to offering the flexibility of choosing the river spreading area, this method is found to be very successful in simulating the surface salinity of the Indian Ocean [Kurian and Vinayachandran, 2006, 2007, Vinayachandran et al., 2012, Behara and Vinayachandran, 2016]. Hence, we have employed a similar method to include the global river discharge in the high-resolution model [Vinayachandran et al., 2022]. The exact location of the river mouth is identified and fixed in the model, for each river. Accordingly, the extent of each river in the ocean is decided based on the magnitude of the river discharge during each month. Spreading zones are chosen such that water supplied to each grid box does not exceed 0.05m/day, a value recommended [Griffies, 2004], to maintain model stability. Thus, the area over which the discharge of a river is distributed depends on the discharge volume. Vertically, the river is discharged in the upper 10 m, which is predetermined in the model such that each layer receives a fraction of the total discharge. The inter-annual monthly river runoff [Dai, 2017] available from 1900 to 2014, is used for river discharge in the model. However, large data gaps existed for many rivers for several years during this period. Hence a monthly climatology was prepared from the available years for each river system. Based on the minimum thickness, global scale, and vertical resolution, the upper 10 m has been chosen for the distribution of runoff.

The model spin-up was carried out using initial conditions for 175 years starting from a

state of rest. Additional experiments branch off for a further 40 years from this spinup. The climatological run (RIVER) with all the major rivers included and a designed experiment where all the rivers (NORIVER) were switched off are utilised to study the impact of rivers on the global ocean. In the present study, we utilise the 40th year, monthly simulations confined to the BoB. The difference plot refers to RIVER minus NORIVER simulation.

Model Sea surface height (SSH) anomaly and AVISO (<https://www.aviso.altimetry.fr/en/data.html>) SSH anomaly shows good agreement. Major features of the SSH anomaly (Figure 1) are simulated well by the model. The Lakshadweep high and low during winter and summer respectively are reproduced by the model and it reproduces the cyclonic low and anticyclonic high in the BoB also remarkably well. Validation of the model for SST, salinity, and currents can be found in Vinayachandran et al. [2022]. The SST variability in the BoB, low salinity plume, and its circulation along the ECI are reproduced by the model reasonably well (see Figure 1 and Figure 2 from Vinayachandran et al. [2022]). The major variability in SST occurs in the northern BoB, southwest coast of India, and northern Arabian Sea and shows a good comparison with observations (Figure 2). Though the salinity standard deviation from the model captures the prominent patterns of variability such as those near the major discharge region in the BOB and the southwest coast of India, the magnitude seems weaker compared to observations. The correlation of model SST with WOA18 [Boyer et al., 2018] SST is above 0.8 over most parts of the basin (last panel, Figure 2). The root mean square error (RMSE) estimates are higher along the southwest coast of India compared to observation. The rest of the regions show errors less than 1°C. In general, the model simulates the general circulation features and thermohaline variability of the north Indian Ocean (Figure 1 and Figure 2. from Vinayachandran et al. [2022]) similar to observations and hence can be used as a tool to study the ocean dynamics in the region.

3 BoB Upwelling Simulation in the Model

The southwest monsoon winds are nearly parallel to the ECI with high strength during June - August period (only July shown, Figure 3) and thus favourable for Ekman type of upwelling. The curl of the wind stress is also positive and favourable for upwelling during the May-September period (only July shown, Figure 3). The cyclonic curl strengthens during June-July along the east coast from around 14°N to 20°N and weakens by August. To quantify Ekman upwelling, the upwelling index (UI) is calculated using the formula $UI = \tau_a / \rho f$ [Bakun, 1975], where τ_a is the alongshore wind stress, ρ is the density of water, and f is the Coriolis force. Positive values of UI indicate upwelling (Figure 4).

As a proxy to represent the upwelling signatures from the ocean, we have calculated the SST index (UI_{sst}) from model simulations. The difference of SST between the coast and at a location 100 km away from the coast at the same latitude following Patel et al. [2020] is considered here as the SST index for upwelling. Thus a positive value of UI_{sst} indicates cooling near the coast which can be used to quantify the upwelling that is realistically taking place in the ocean.

Temporal variability of UI calculated for the ECI at the selected location from 19° to 12°N are presented in Figure 4 (second row, monthly smoothed). The wind-driven upwelling starts in February and is positive (maximum of $1.2 \text{ m}^2 \text{ s}^{-1}$) for all locations along the coast till September except at 12°N, the southernmost location (purple line, upper and lower panel, Figure 4), which becomes positive from May onwards and is higher than that at the other location for the summer monsoon period. The UI_{sst} (upper panel, Figure 4) is positive (maximum of $1.2 \text{ }^\circ\text{C}$) suggesting upwelling from February till September. High positive values that begin to appear in June indicate the presence of upwelling during the summer monsoon and it decreases rapidly during October.

The EICC as seen in the OSCAR data set (first row, Figure 5) flows northward upto about 17°N during the month of June and then turns offshore. The inshore region of this offshoot shows a cyclonic eddy with equatorward flow close to the coast. With the progress in the summer monsoon, the northward flow weakens and the equatorward flow gets established along the northern half of the coast. The cyclonic eddy persists during June - August but weakens in September. The model EICC (second row, Figure 5) is consistent with the OSCAR. The equatorward flow in the northern section of the coast and the poleward flow seaward of it are well reproduced by the model. The major difference is seen in the model EICC in the southern sector of the coast which flows more in the offshore direction than in the OSCAR data set. The model simulation offers a good comparison with the SSH anomaly from AVISO (5th and 6th row, Figure 5). SSHA is higher in the entire western bay during June which changes signs towards the end of the season. A low sea level corresponding to the cyclonic eddy is noticed around 18°N near the coast. The formation of this eddy occurs a while later in the model but the alternating bands of low and high sea levels corresponding to the circulation (5th and 6th row, Figure 5) is in good agreement with the altimetry.

In order to show the cooling associated with upwelling along the ECI during the summer monsoon months of June, July, August, and September, the SST from the model (RIVER) simulation and WOA18 are utilised and their difference from May are shown (first two rows, Figure 5). In June, close to the coast, northwestern bay (till 18°-20°N) shows warming (0.5-1°C) while the southwestern bay cooling with respect to May (Figure 5). Both model and data show warming in the northern part of the coast (north of 18°N) and cooling in the southern part due to the monsoon. In July and August, the northern bay continues to show warming compared to May which becomes more pronounced and extends southward in September. The SST cooling in the south increases during July and August (1-2°C). Thus both the model and observation imply an increase in SST cooling south of 18°N during the summer monsoon associated with

upwelling. The strength of upwelling shows considerable latitudinal variation along the coast within the season with a noticeable impact on the vertical structure. Figure 6 shows the latitude depth section of temperature and salinity along the ECI (along the 100m isobath) from 10°- 20° N from May to October. Prior to the summer monsoon, the coastal region to the south of 16 °N exhibits higher temperatures (29°C) at the surface. With the start of the summer monsoon in June, the isotherms rise by about 30 to 50 m compared to their pre-monsoon position in these southern parts. In the north, however, there is a deepening of similar magnitude during the same period. SST is also maintained above 28°C in the north and drops to 27°C in the south during the summer monsoon. Another interesting feature noticed here is the sudden increase in the upper layer temperatures (28°C) from July to August south of 15°N. This corresponds well with the UI and UI_{SST} , which also shows a slight decrease in its magnitude during August (Figure 4). Local alongshore winds apparently slow down during August (Figure not shown). Breaks in upwelling were noticed in a recent study using high-frequency HF radar data [Dey and Sil, 2023] where they associated it with the local wind variability.

Beginning in June, a low salinity plume (< 2 psu) expands southward from the northwest bay and it reaches 16°N in September (3rd and 4th row, Figure 5). The pattern is similar in the model with the low salinity values slightly less than that of observations. In contrast, there is an increase in salinity to the south of 18°N which can be attributed to the upwelling of high salinity water near the coast [Shetye et al., 1991]. A freshwater plume progressively moves southward along the coast along with an increase in the vertical extent (3rd and 4th row, Figure 6). The salinity increases near the surface due to upwelling in June but decreases thereafter due to the southward flow of freshwater. Higher temperatures are maintained at the northern parts of ECI, where low salinity values are found, along with thinning of the mixed layer (Figure not shown). By the end of October, the low saline values (less than 34 psu) spread along the entire coast.

Cross-shore vertical section (Figure 7) taken perpendicular to the coast till 300 km in the horizontal and 200 m vertically was selected to illustrate the variations in temperature, salinity, vertical velocity, density, and currents during upwelling at three different locations along the ECI; one each in the south (12°N), center (16°N), and north (18°N). In the upper 60 m, isotherms are inclined upward near the coast, indicating upwelling (1st row, Figure 7). Temperatures cool maximum to the south (26°C, at 12° and 16°N) compared to the north (27°C, 18°N) in the upper layers close to the coast. Downwelling is noticed below 60 m near the coast with the isotherms doming downwards consistent with observations [Shetye et al., 1991] in this region. The northernmost station shows the lowest salinity (18°N, 34 psu) with values increasing southward. Even though low salinity water is present in the upper layers, upwelling tends to bring saltier water from beneath to the surface near the coast (second row, Figure 7). Vertical velocity is upward (positive) (3rd row, Figure 7) at all three locations in the upper layers especially near the coast. Density decreases offshore (22 Kg/m³, 4th row, Figure 7) whereas upwelling brings comparatively denser waters to the top near the coast at all the locations. The cross-shore deflection of currents to the right is apparent up to a distance of 50-100 km (vectors, 4th row, Figure 7) at the surface. These currents turn clockwise with depth and reverse at a depth of about 30-40 m completing a clockwise circulation.

In summary, the high-resolution ocean model realistically simulates the upwelling that occurs along India's east coast through the summer. The alongshore wind stress-based UI showed upwelling starting from February and lasting till September. The model-based UI_{sst} displayed the model's ability to capture the upwelling response from the ocean. The surface winds favouring upwelling along the east coast of India produce a differential upwelling pattern north and south of 18°N in the western bay. This is in accordance with the currents which have a poleward component south of 18°N and equatorward north of it. The SST cooling associated with upwelling increases as one moves south, where the effects of the low salinity plume from the

northern bay are less prominent and high salinity water (35 psu) slopes up. The western bay cools more to the south of 18°N and warms north of it with respect to the month of May. The warming becomes more pronounced and extends southward by September. There is a break in the strength of upwelling during August, south of 16°N, when the temperature starts increasing corresponding to the weakening of the wind stress curl in the region. The upwelling is noticed till a depth of 60 m in the vertical and through this process, higher salinity denser water reaches the surface. The cross-shore response of current [Dey and Sil, 2023], typical of upwelling is evident in the region upto a distance of about 50-100 km offshore.

4 Impact of river runoff on upwelling

Low salinity water is evident in the northwestern bay which intensifies as the monsoon progresses. However, towards the southwestern bay (south of 18°N), the low salinity plume (<33 psu) becomes prominent after August (Figure 6). A low salinity plume has been reported to suppress upwelling in the northwestern bay [Shetye et al., 1991, Behara and Vinayachandran, 2016, Thushara and Vinayachandran, 2016]. These factors prompted us to investigate the response of upwelling to river runoff in this region. In this section, the role of rivers in upwelling is explained using the model experiments with the inclusion and exclusion of river runoff into the ocean. To identify the river impact on SST, salinity, currents, MLD, and SSH, we present the spatial maps of differences between NORIVER and RIVER simulations (Figure 8). A lateral and vertical cross-shore section of temperature and salinity difference is also used to show the variations induced by rivers in the vertical and cross-shore directions (Figure 9 and Figure 10).

The salinity difference between RIVER and NORIVER defines the course taken by river water in the BoB (seen as negative values in Figure 8, 1st column). The river water spreads from the northern bay starting in June and has the highest values present in the head bay during

August (3 psu). The currents circulate these waters inside the bay (vectors, 1st column, Figure 8). The EICC transports it equatorward to the tip of India during the northeast monsoon (see January in Figure 8), while the WICC carries it northward along the west coast of India [Vinayachandran et al., 2022]. The EICC strengthens equatorward (southward arrows, 1st column, Figure 8) with the inclusion of rivers along the east coast. A negative difference in MLD (3rd column, Figure 8) implies shallowing in the northwestern bay with the inclusion of rivers during August which spreads southward and shows maximum shoaling along the path of the EICC during January. The positive SSH (4th column, Figure 8) represents an increase in sea level across the entire bay and along the east coast when rivers are included.

The northwestern bay shows a positive SST difference specifying warming in the presence of rivers ($>0.5^{\circ}C$), during June which apparently shifts southward along with the transport of river water (1st and 2nd column, Figure 8). The offshore spread of warmer SST anomalies is associated with more robust offshore differences in currents (vectors, 1st column for August in Figure 8). The SST and current differences (1st and 2nd column, Figure 8) show a clockwise recirculation of warmer water back to the eastern coast. Thus the inclusion of rivers appears to be the reason for warming or the suppression of upwelling-induced cooling along the east coast. Meanwhile eastern bay cools during most of the period. In a similar experiment but by keeping the air-sea fluxes constant, Behara and Vinayachandran (2016) noticed warming in excess of $1^{\circ}C$ in the northwestern bay and attributed it to the air-sea fluxes over a thin mixed layer owing to stratification from river and rain. The UI_{sst} , a measure of upwelling in the ocean described in section 3 (dash curve, top panel, Figure 4) is higher for the NORIVER than RIVER at all the locations. This is an additional indication that the weakened stratification in the absence of rivers strengthens upwelling and increases the cooling associated with upwelling along the east coast of India. Northern parts ($18^{\circ}N$) record the maximum SST difference ($>0.5^{\circ}C$) owing to rivers (1st row, Figure 9) during June/July compared to the south. The difference in SST

indicates warming decreases offshore but persists till October with the inclusion of rivers. The warming caused by rivers extends vertically (1st row, Figure 10) up to 100-120 m near the coast. The negative salinity difference implies freshening in the region which increases with the progress in monsoon and peaks during post-monsoon (in October, 2nd row, Figure 9) in the presence of rivers. The highest difference occurs towards the north (> 3 psu) gradually decreasing towards the south. Owing to the presence of rivers, the salinity decreases offshore (2nd row, Figure 9) over a distance of more than 150-300 km and vertically till 60 m in the south increasing to 120 m in the north (at 18°N, Figure 10).

In general, warmer anomalies in the presence of rivers are noticed over regions where salinity decreases owing to rivers. The river discharge into the head bay during June and July is confined to the northwestern bay (1st column, Figure 8) making the region fresher and highly stratified. The outflow of low saline water from the bay along the ECI south of 18°N starts with the southward strengthening of the EICC (see section 3 about EICC, Figure 5) later in August/September. Fresher stratified water due to rivers in the northern parts induces more warming and suppresses upwelling during the initial parts of the monsoon itself. This also explains the differential cooling during upwelling between north and south of 18° N noticed in section 3 (1st row and 2nd row, Figure 5) where the northern part warms and the southern region cool. When rivers are switched off, the salinity increases in the northern parts of the ECI which is reflected in the temperature as it cools more associated with upwelling (Figure 9 and Figure 10).

In summary, the river runoff tends to warm the northern bay, and this warming spreads along the ECI towards the south. Rivers cause EICC to strengthen, decrease the salinity by more than 3 psu, cause MLD to shallow along the EICC's course, and raise the sea level. In general, the southern parts of the western bay experience more upwelling-related SST cooling than the northwestern bay during the summer monsoon along the east coast (Figure 6 and

Figure 7). Comparatively warmer temperatures, owing to rivers observed in the northwestern bay occurs over regions of low salinity and are observed to move southward together. With the exclusion of rivers, the cooling from upwelling becomes stronger north of 16°N where salinity is higher now (Figure 9). Without rivers, the vertical extent of upwelling increases in the western bay (100 m). Horizontally, the impact of rivers in warming is noticed upto 300 km offshore (Figure 10).

5 Processes and Mechanisms

The upper layers of the bay are highly stratified owing to low salinity caused by the huge river discharge and enormous rainfall [Shetye et al., 1991, Vinayachandran et al., 2002].

In this section, we explore the processes causing the variability in upwelling in the western bay associated with the river discharge impacted by stratification. This is carried out by examining Brunt Vaisala frequency N^2 (T,S) along the ECI during the upwelling period.

5.1 Impact of rivers on stratification

The impact of salinity on the stratification can be studied by separating the thermal (T) and haline (S) effects of N^2 [Maes, 2008, Maes and O’Kane, 2014]. Computations are carried out using the following equations.

$$N^2(T,S) = (g/\rho) d\rho/dz$$

$$N^2(T,S) = N^2(T) + N^2(S)$$

$$\text{where } N^2(T) = (g\alpha) dT/dz$$

$$N^2(S) = N^2(T,S) - N^2(T)$$

$$\text{where } , \alpha = (-1/\rho)d\rho/dT$$

T, S, and z represent temperature, salinity, and depth respectively. α represents the thermal

expansion coefficient, g represents gravity, and ρ represents density. Ocean salinity stratification (OSS) is then defined as the average of positive $N^2(S)$ from the surface to 300 m [Maes and O’Kane, 2014]. The difference between the OSS of RIVER and NORIVER is used from May through October to quantify the impact of rivers on salinity stratification (Figure 11). Positive difference in Figure 11 indicates northern bay is stratified with respect to salinity when rivers are included. Major rivers such as Ganga, Brahmaputra, Irravady, Kaveri, and Krishna discharge into the basin as the summer monsoon progresses and OSS starts increasing from June (> 0.2 cph) spreading southwards along the ECI. By September, the highest values occur till 18°N , extending further south till the Sri Lankan region in October. Higher salinity stratification north of 18°N in September corresponds to the weaker upwelling regimes in the northwestern bay. When rivers are absent, this stratification is weaker, which promotes the mixing of the upper oceanic layers by wind-driven turbulence and vertical ocean processes.

The variability in stratification with latitude and depth along the east coast and the relative contribution of $N^2(T,S)$ and $N^2(S)$ is presented in Figure 12. As early as May and extending till July, the upper 60 m values of $N^2(T,S)$ are higher indicating stratification, which intensifies from August, associated with monsoon and river discharge (1st three columns in 1st and 2nd row, Figure 12). $N^2(S)$ (Last three columns in 1st and 2nd row, Figure 12) on the other hand starts increasing in July in the north where huge discharge from Ganga, Brahmaputra, and major rivers occur and also between 15° and 17°N owing to a river discharge from Krishna in the model. The highest values occur in the upper layers above 20 m which progressively grow laterally and vertically displaying the stratification in the region induced by low salinity from rivers. In October, the upper layers become highly stratified till 13°N while a secondary maximum occurs north of 16°N extending vertically to 60 m. The positive values in the difference plot (last two rows, Figure 12) show the effect of rivers on stratification. It is very much similar for $N^2(T,S)$ and $N^2(S)$, suggesting the major contribution to stratification in this region is from

rivers ($(N^2(S))$) where salinity plays a major role. Higher stratification owing to rivers noticed north of 16°N slowly extends southwards with depth after August. The major contribution for the double maximum in stratification with depth north of 16°N in October is associated with river discharge.

Therefore, the lower salinity associated with river discharge is the reason for the enhanced stratification during the summer monsoon and post-monsoon in the upper layers along the ECI, particularly in the northern parts. During the pre-monsoon to early monsoon period (1st three columns, Figure 12) higher stratification in the upper 60 m is contributed by temperature term as well while the salinity stratification (last three columns, Figure 12) increases southwards along the east coast starting from August.

The upper layers of the western bay are generally highly stratified depending on temperature and salinity and stratification rapidly increases from August as the salinity term starts dominating due to the increase in the river discharge. The higher stratification is prominent in the upper layers till 16°N in September implying that the effect of stratification is higher in the northern parts during the summer monsoon. Stratification owing to rivers extends to the southern parts of ECI later in October. As observed, along the ECI, upwelling-induced cooling increases towards the south (Figure 6). The local wind forcing which triggers upwelling has to work against the stratification induced by rivers in the northern parts, during the monsoon season. The contribution of salinity stratification gets weaker towards the south which leads to increased cooling to the south associated with upwelling. This produced a differential cooling pattern between the northern and southern parts described earlier. The scenario changes when rivers are switched off, stratification weakens in the northern parts, and cooling due to upwelling becomes maximum in this region. The cooling generated by upwelling increases by almost $0.5^\circ\text{-}1^\circ\text{C}$ in the northern bay, with amplitude decreasing southwards (Figure 9 and Figure 10). This confirms that the salinity stratification from rivers during the summer monsoon

is one reason that reduces the cooling produced by upwelling in the northwestern bay, the effect of which decreases southwards along the coast. The weaker stratification caused by the absence of rivers resulted in increased cooling associated with upwelling as it is easier for the subsurface water to rise to the top. Cooler water rises from a depth of 100 m instead of 60 m (noticed in Shetye et al. [1991]) when rivers are excluded (Figure 10). The difference in stratification due to rivers being higher in the northern parts in July-September compared to southern locations suggest that rivers inhibit upwelling in the northwest bay during the summer monsoon.

6 Summary and conclusion

East coast of India upwelling is a seasonal phenomenon, occurring due to the seasonal monsoon winds and currents [Shetye et al., 1991, Thushara and Vinayachandran, 2016] which push water away from the coast allowing nutrient rich and cooler water from the depth to rise to the surface layers. BoB receives abundant rainfall and river discharges during the summer monsoon decreasing the salinity and increasing the stratification in the region. Using a high-resolution OGCM configured for the global ocean, the upwelling along the ECI was studied. The model simulated the cooling associated with upwelling along the ECI reasonable well. The UI shows favourable conditions for upwelling beginning from February along the ECI with values ranging between 0.6 -1.2 m^2s^{-1} . An SST based UI index (UI_{sst}) and UI serve as good indicators of upwelling along the ECI. The SST cooling in the western bay due to upwelling shows a differential pattern north and south of 18°N with higher cooling in the south. The cooling was less in the northern parts, where salinity influence from rivers was maximum. The currents were directed poleward south of 18°N and equatorward north of it in concurrence with the observed differential cooling. With the progress in the monsoon, the freshwater plume, the warmer SST, and the coastal current strengthen. The warmer waters occur over low salinity water and extend

deeper in the northern parts of the ECI in the vertical compared to the southern parts. With the expansion of the freshwater plume southward and vertically, the warmer layers grew thicker equatorward. In the vertical, upwelling is noticed till 60 m with downwelling occurring below it. During upwelling, high saline water is pumped upwards from beneath, making the upper layer more saline before the arrival of fresher water from the northern bay. Low salinity water inhibits cooling associated with upwelling. In order to study the impact of rivers on upwelling two experiments were carried out; one with rivers and the other without rivers.

The difference between the RIVER and NORIVER simulations was then used to isolate the river impact on the ECI upwelling. The salinity drops more than 3 psu in the head bay due to rivers and the river water flows along the east coast equatorward. The presence of rivers cause the western bay to warm (around 0.5°C) and these anomalies propagate southwards along with the low saline water. As the river water spreads southward from the northern bay, the EICC strengthens, MLD shoals and SSH rises along the east coast of India. The UI_{sst} , from the ocean, is higher for the NORIVER along the ECI implying weaker stratification in the region due to high saline waters enhances upwelling. In general, when rivers are present upwelling related cooling increases southwards (from 27°C in the north to 26°C in the south). The river runoff suppresses cooling associated with upwelling, which is observed as the warming anomalies first noticed in the northwestern bay, which slowly propagates southwards along with the low salinity water. The exclusion of rivers causes increased cooling associated with upwelling in the northern parts while the vertical extent increases by 40 m along the ECI close to the coast.

The stratification caused by salinity was examined by separating the thermal and haline effects from $N^2(T, S)$ and by defining the OSS as the average of $N^2(S)$ in the upper 300 m. The difference in OSS between the RIVER and NORIVER experiments highlights the influence of rivers on stratification. The OSS increases along the ECI with the river discharge, indicating that the region's stratification depends on river runoff. $N^2(T, S)$ in the upper layers shows

that salinity stratification increases from August and expands southwards with depth. The variability of $N^2(S)$ with depth suggests that the upper layers of the northwestern bay are highly stratified where the influence of rivers is higher. As a result, during the summer monsoon, the rivers suppress cooling in the northwest bay than the south. When rivers are not included, higher salinity and weakened stratification result in increased cooling along the path of river flux during the summer monsoon.

In summary, during the summer monsoon, rivers promote increased warming in the northwestern bay, suppressing cooling caused by upwelling through increased stratification. Stratification by rivers emerges as the major factor suppressing ECI upwelling particularly in the northern parts. The Local winds and remote forcing from the equator dominate the sea-level cycle and associated upwelling processes in the BoB through propagating waves and eddies [Shankar et al., 2002]. The equatorial wind stress forced upwelling Kelvin wave trigger upwelling in the northwest bay [Ray et al., 2022]. The termination of upwelling in the northern bay after June is again associated with the arrival of downwelling coastal trapped Kelvin wave [Ray et al., 2022, Dey and Sil, 2023]. The influence of rivers on the coastally trapped Kelvin waves from the head bay and along the ECI has important implications on upwelling along the ECI. Because of the fact that monthly data is not sufficient for tracking of propagating coastal waves, this part of the analysis has not been addressed here.

Acknowledgements Model simulations used in the study were carried out under the O-MASCOT project funded by INCOIS, Ministry of Earth Sciences, Govt. of India. Simulations were carried out on the MIHIR supercomputer at NCMWRF, Ministry of Earth Sciences, Govt. of India. PNV acknowledges partial financial support from J C Bose Fellowship, DST, Govt. of India, and National Supercomputing Mission, DST, Govt. of India. The model used in this study is version 5 of the modular ocean model (MOM5p1) developed at the National Oceanic and Atmospheric Geophysical Fluid Dynamics Laboratory (NOAA/GFDL). We thank AVISO

(<https://www.aviso.altimetry.fr/en/data.html>) for the SSH data and WOA18 [Boyer et al., 2018] for the Salinity and Temperature data. Ferret has been used for data analysis and graphics.

References

- P. Amol, P. Vinayachandran, D. Shankar, V. Thushara, V. Vijith, A. Chatterjee, and A. Kankonkar. Effect of freshwater advection and winds on the vertical structure of chlorophyll in the northern Bay of Bengal. *Deep Sea Research Part II: Topical Studies in Oceanography*, 179:104622, 2020. ISSN 0967-0645. doi: <https://doi.org/10.1016/j.dsr2.2019.07.010>. URL <https://www.sciencedirect.com/science/article/pii/S0967064518301218>. The Second International Indian Ocean Expedition (IIOE-2): Motivating New Exploration in a Poorly Understood Ocean Basin Volume 3.
- A. Bakun. *Daily and weekly upwelling indices, west coast of North America, 1967-73*, volume 693. Department of Commerce, National Oceanic and Atmospheric Administration . . . , 1975.
- A. Behara and P. N. Vinayachandran. An OGCM study of the impact of rain and river water forcing on the Bay of Bengal. *Journal of Geophysical Research*, 121:2425–2446, 2016.
- T. P. Boyer, H. E. García, R. A. Locarnini, M. M. Zweng, A. V. Mishonov, J. R. Reagan, K. A. Weathers, O. K. Baranova, C. R. Paver, D. Seidov, et al. World Ocean Atlas. *NOAA National Centers for Environmental Information*, 2018. URL <https://www.ncei.noaa.gov/archive/accession/NCEI-WOA18>.
- A. Dai. Dai and Trenberth Global River Flow and Continental Discharge Dataset, 2017. URL <https://doi.org/10.5065/D6V69H1T>.

- S. Dey and S. Sil. Spatio-temporal variability of coastal upwelling using high resolution remote sensing observations in the Bay of Bengal. *Estuarine, Coastal and Shelf Science*, 282:108228, 2023. ISSN 0272-7714. doi: <https://doi.org/10.1016/j.ecss.2023.108228>. URL <https://www.sciencedirect.com/science/article/pii/S0272771423000185>.
- S. M. Griffies. *Fundamentals of Ocean Climate Models*, Princeton University, 2004.
- R. R. Hood, L. E. Beckley, and J. D. Wiggert. Biogeochemical and ecological impacts of boundary currents in the Indian Ocean. *Progress in Oceanography*, 156:290–325, 2017.
- B. Johns, A. D. Rao, and G. S. Rao. On the occurrence of upwelling along the East Coast of India. *Estuarine, Coastal and Shelf Science*, 35(1):75–90, 1992. doi: 10.1016/s0272-7714(05)80057-5.
- J. Kämpf and P. Chapman. *Upwelling systems of the world*. Springer, 2016.
- J. Kurian and P. N. Vinayachandran. Formation mechanisms of temperature inversions in the southeastern Arabian Sea. *Geophysical Research Letters*, 331, Sept. 2006. doi: 10.1029/2006GL027280.
- J. Kurian and P. N. Vinayachandran. Mechanisms of formation of the Arabian Sea mini warm pool in a high resolution OGCM. *Journal of Geophysical Research*, 112, May 2007. doi: 10.1029/2006JC003631.
- W. G. Large and S. G. Yeager. The global climatology of an interannually varying air–sea flux data set. *Climate dynamics*, 33(2):341–364, 2009.
- W. G. Large, J. C. McWilliams, and S. C. Doney. Oceanic vertical mixing: A review and a model with a nonlocal boundary layer parameterization. *Reviews of Geophysics*, 32(4): 363–403, 1994. doi: <https://doi.org/10.1029/94RG01872>.

- C. Maes. On the ocean salinity stratification observed at the eastern edge of the equatorial Pacific warm pool. *Journal of Geophysical Research: Oceans*, 113(C3), 2008.
- C. Maes and T. J. O’Kane. Seasonal variations of the upper ocean salinity stratification in the Tropics. *Journal of Geophysical Research: Oceans*, 119(3):1706–1722, 2014.
- S. Patel, M. Vithalpura, S. K. Mallick, and S. Ratheesh. Temporal and Spatial Variations of Monsoonal Upwelling along the South West and East Coasts of India. *Marine Geodesy*, 43(4):414–432, 2020. doi: 10.1080/01490419.2019.1703061.
- A. Rao, S. Dube, and P. Sinha. Numerical modelling of coastal upwelling in the Bay of Bengal. *Environment international*, 21(5):667–670, 1995. doi: [https://doi.org/10.1016/0160-4120\(95\)00077-X](https://doi.org/10.1016/0160-4120(95)00077-X).
- R. Rao, M. Girish Kumar, M. Ravichandran, A. Rao, V. Gopalakrishna, and P. Thadathil. Interannual variability of Kelvin wave propagation in the wave guides of the equatorial Indian Ocean, the coastal Bay of Bengal and the southeastern Arabian Sea during 1993–2006. *Deep Sea Research Part I: Oceanographic Research Papers*, 57(1):1–13, 2010. ISSN 0967-0637. doi: <https://doi.org/10.1016/j.dsr.2009.10.008>. URL <https://www.sciencedirect.com/science/article/pii/S0967063709002003>.
- T. Rao, D. P. Rao, B. P. Rao, and V. Raju. Upwelling and sinking along Visakhapatnam coast. *Indian Journal of Marine Sciences*, 15:84–87, 1986.
- T. N. Rao. Spatial distribution of upwelling off the central east coast of India. *Estuarine, Coastal and Shelf Science*, 54(2):141–156, 2002. doi: doi:10.1006/ecss.1999.0835.
- T. N. Rao and B. P. Rao. Alongshore velocity field off Visakhapatnam, east coast of India during premonsoon season. *Indian J Mar Sci*, 1989.

- S. Ray, D. Swain, M. Ali, and M. Bourassa. Coastal Upwelling in the Western Bay of Bengal: Role of Local and Remote Windstress. *Remote Sensing*, 14, 09 2022. doi: 10.3390/rs14194703.
- D. Shankar, P. Vinayachandran, and A. Unnikrishnan. The monsoon currents in the north Indian Ocean. *Progress in Oceanography*, 52(1):63–120, 2002. ISSN 0079-6611. doi: [https://doi.org/10.1016/S0079-6611\(02\)00024-1](https://doi.org/10.1016/S0079-6611(02)00024-1). URL <https://www.sciencedirect.com/science/article/pii/S0079661102000241>.
- S. Shetye, S. Shenoi, A. Gouveia, G. Michael, D. Sundar, and G. Nampoothiri. Wind-driven coastal upwelling along the western boundary of the Bay of Bengal during the southwest monsoon. *Continental Shelf Research*, 11(11):1397–1408, 1991.
- B. Sindhu, I. Suresh, A. Unnikrishnan, N. Bhatkar, S. Neetu, and G. Michael. Improved bathymetric datasets for the shallow water regions in the Indian Ocean. *Journal of Earth System Science*, 116(3):261–274, 2007.
- V. Thushara and P. N. Vinayachandran. Formation of summer phytoplankton bloom in the northwestern Bay of Bengal in a coupled physical-ecosystem model. *Journal of Geophysical Research: Oceans*, 11 2016. doi: 10.1002/2016JC011987.
- P. N. Vinayachandran and R. S. Nanjundiah. Indian Ocean sea surface salinity variations in a coupled model. *Climate dynamics*, 33(2):245–263, 2009.
- P. N. Vinayachandran, V. S. N. Murty, and V. Ramesh Babu. Observations of barrier layer formation in the Bay of Bengal during summer monsoon. *Journal of Geophysical Research*, 107, 2002. doi: 10.1029/2001JC000831.
- P. N. Vinayachandran, C. P. Neema, S. Mathew, and R. Remya. Mechanisms of summer in-

traseasonal sea surface temperature oscillations in the Bay of Bengal. *Journal of Geophysical Research: Oceans*, 117(C1), 2012.

P. N. Vinayachandran, Y. Masumoto, M. Roberts, J. Huggett, I. Halo, A. Chatterjee, A. Prakash, G. Gupta, A. Singh, A. Mukherjee, S. Prakash, L. Beckley, E. Raes, and R. Hood. Reviews and syntheses: Physical and biogeochemical processes associated with upwelling in the Indian Ocean. *Biogeosciences*, 18:5967–6029, 11 2021. doi: 10.5194/bg-18-5967-2021.

P. N. Vinayachandran, C. P. Neema, A. Chatterjee, and S. Prerna. Fate and impact of Bay of Bengal rivers in an intermediate resolution ocean model. In *OCEANS 2022-Chennai*, pages 1–8. IEEE, 2022.

7 Figures

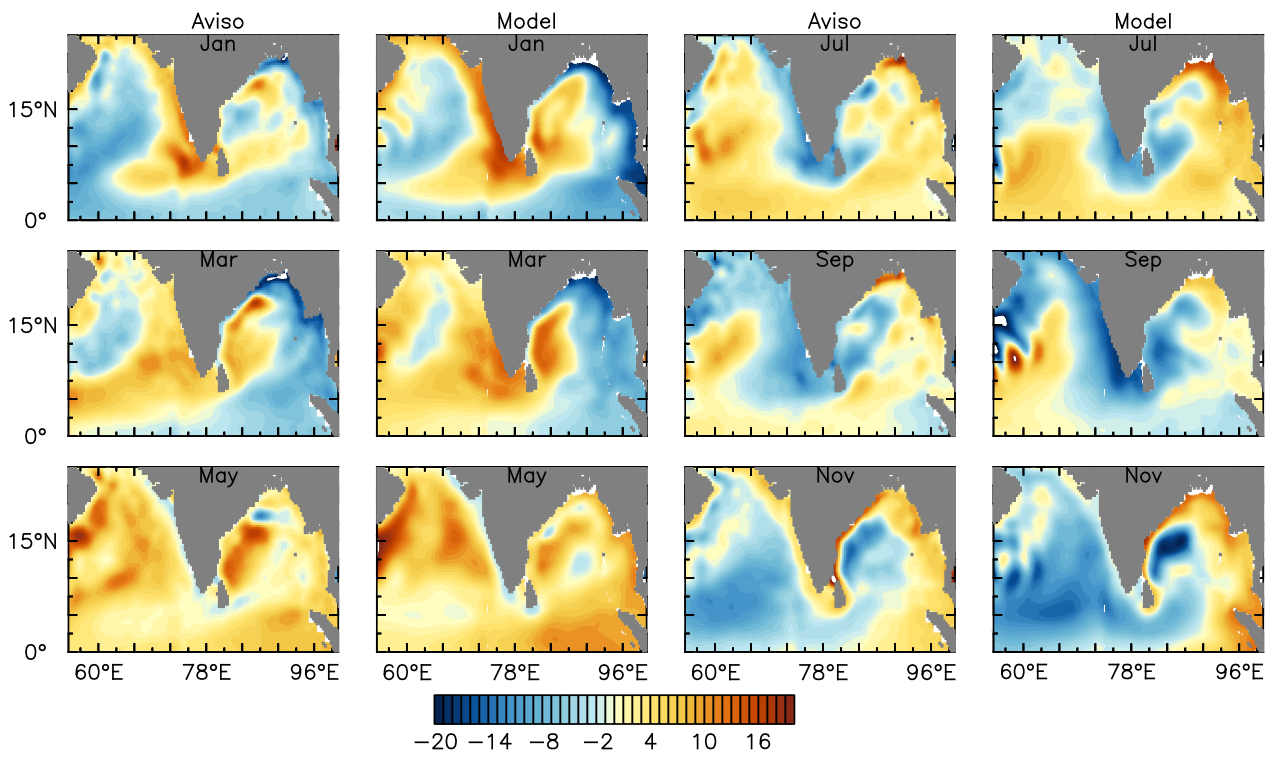


Figure 1: Bimonthly climatology maps of SSH (cm) anomalies from the model (RIVER run) and AVISO.

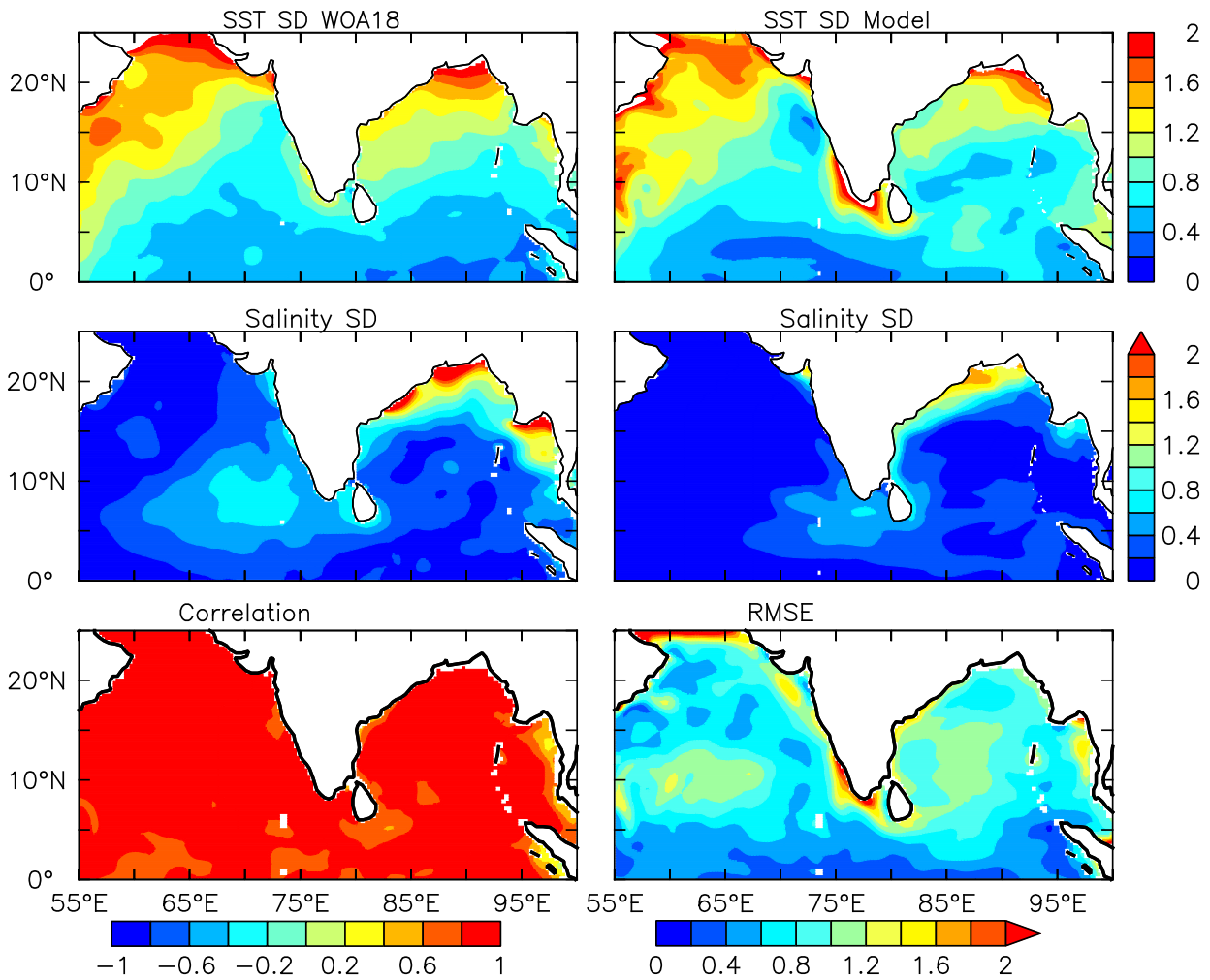


Figure 2: Annual standard deviation for SST (upper panel), and Salinity (middle panel) from WOA18 (left panel) and model (right panel). Bottom panel shows the correlation (left) and RMSE (right) between the model and WOA18 SST. The model results are from the RIVER run.

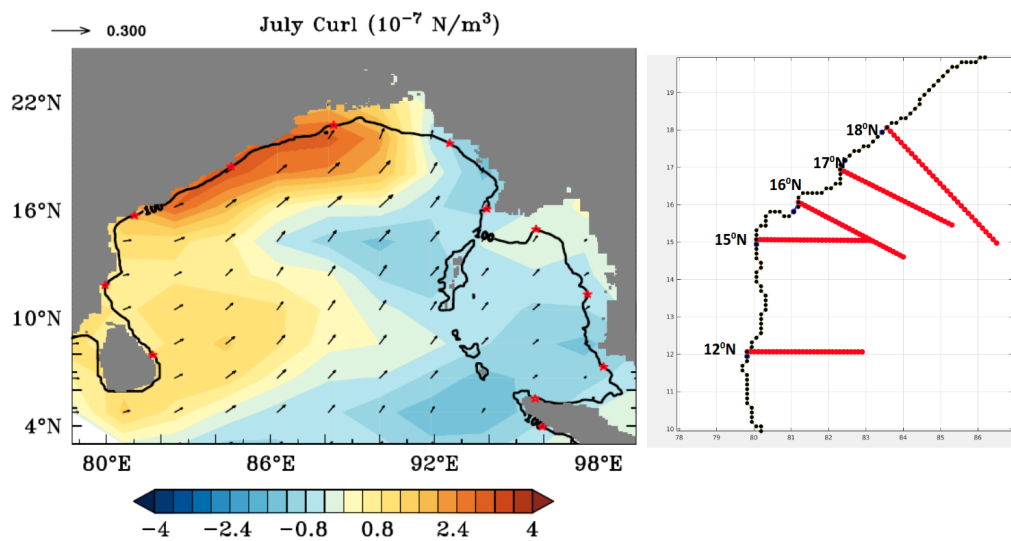


Figure 3: Left panel. Climatological wind stress (vectors, m/s) and curl (shading) calculated from CORE II [Large and Yeager, 2009] 6 hourly data for the month of July. Contour represents the 100 m isobath used in the model. Right panel. The coastal stretch (black line) considered for Figure 6, Figure 12 and sections (red lines) for Figures 7, 9, and 10. The latitude of the section at the coast is marked in the figure.

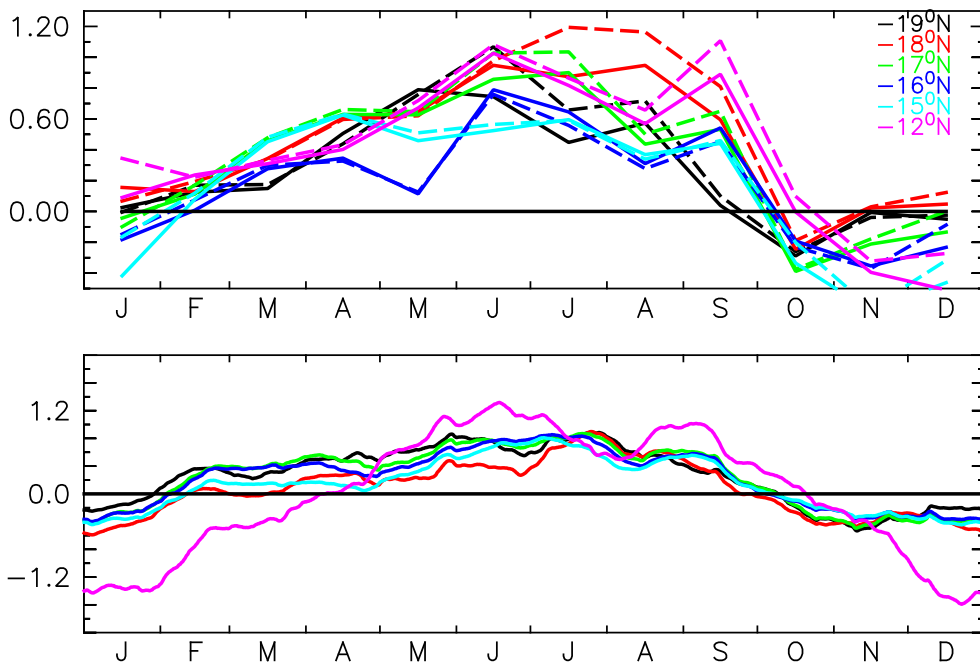


Figure 4: Upwelling Index (UI_{sst}) computed from SST difference from the coast and 1-degree latitude away from the coastal point along the east coast of India (upper panel). Solid curves represent the UI_{sst} from RIVER and dashed ones from NORIVER respectively. Upwelling index computed from alongshore wind stress (UI, bottom panel).

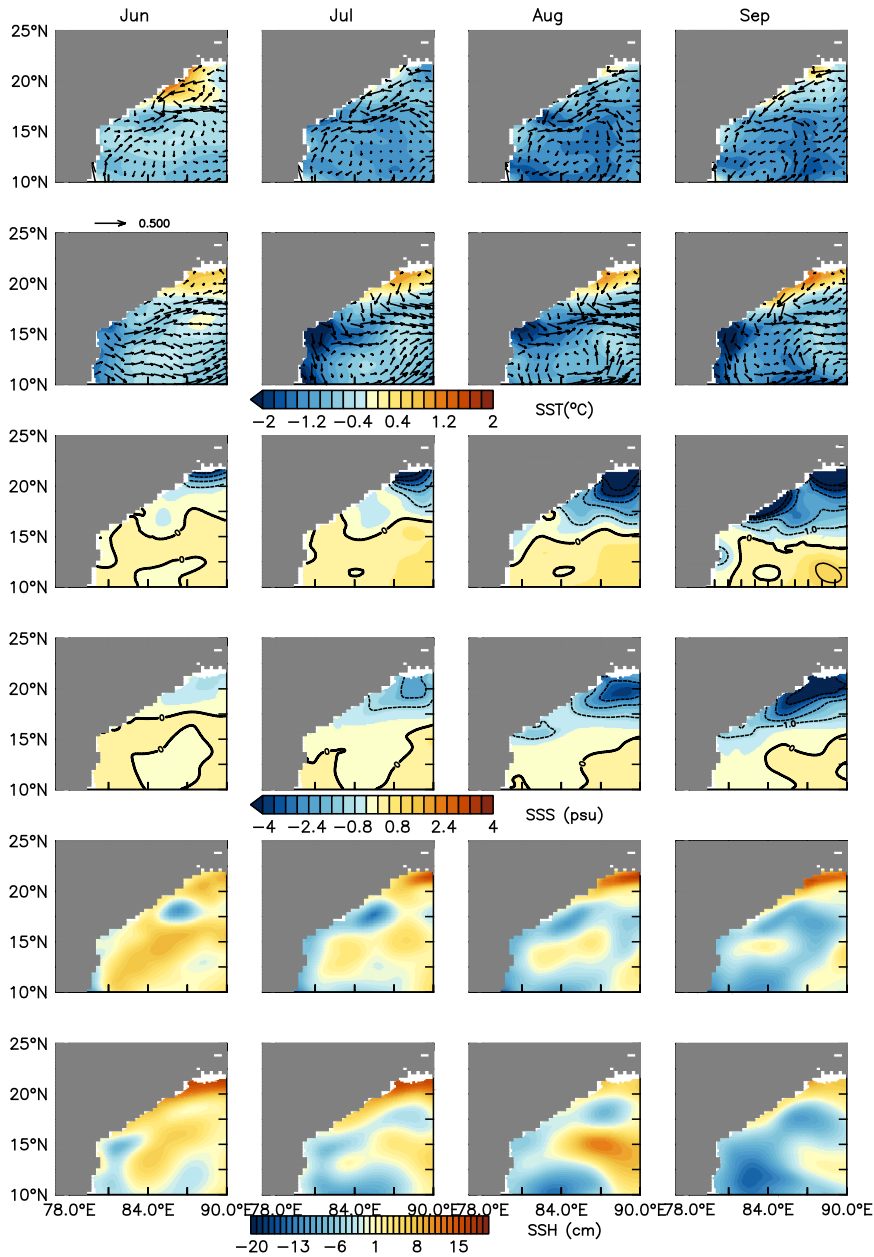


Figure 5: Row 1. Monthly mean currents (vectors, m s^{-1}) from OSCAR and the difference in SST (shading) from that for the month of May from WOA18 (top panel). Row 2. Same as in Row 1 except that current and SST differences are from the model. Row 3. The difference in WOA18 salinity from that for the month of May. Row 4. Same as in Row 3 except that differences are from Model. Row 5. SSH from AVISO and Row 6. SSH from Model for the summer monsoon period. The model results are from the RIVER run.

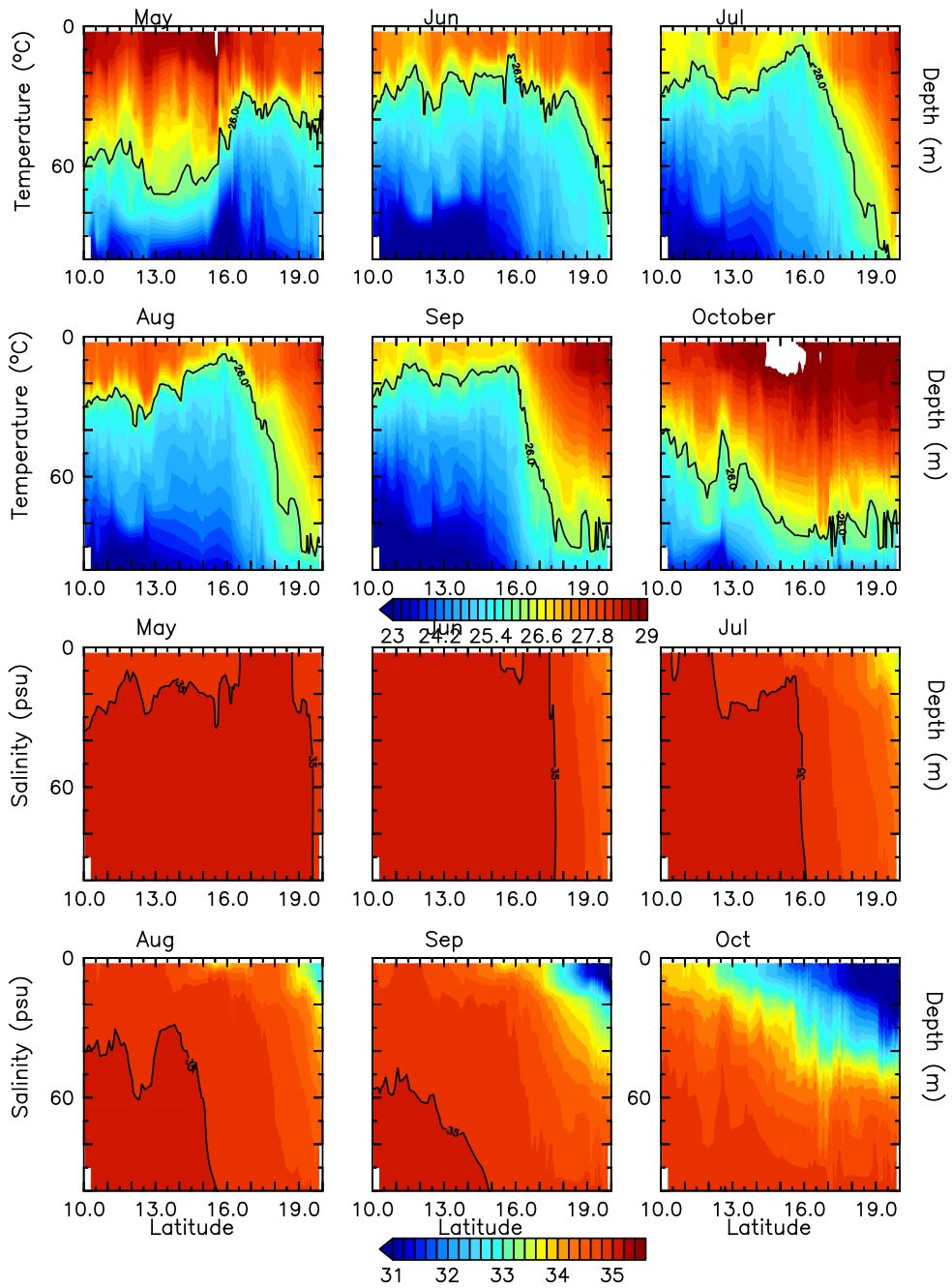


Figure 6: Vertical structure of Temperature (first and second rows) and Salinity (third and fourth rows) along the 100 m isobath of the part of the coastline shown in the right panel of Figure 3 from May-October. The contour marked on the temperature plot is 26°C and on salinity is 35 psu. All results are from the RIVER run.

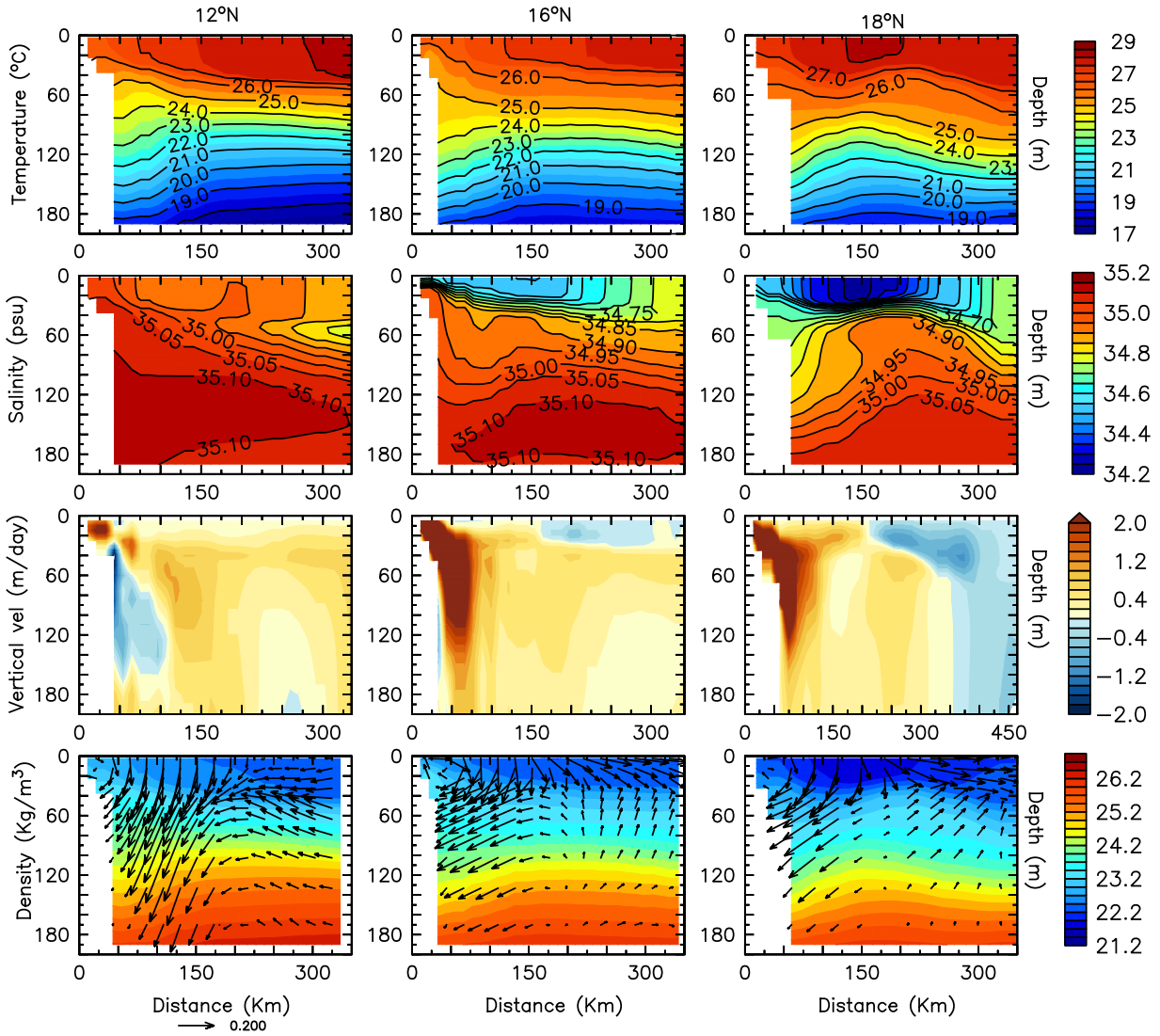


Figure 7: Vertical structure of Temperature (1st row), Salinity (2nd row), and Vertical velocity (3rd row) for the month of July for the sections marked at 12°N, 16°N and 18°N in the right panel of Figure 3. All results are from the RIVER run.

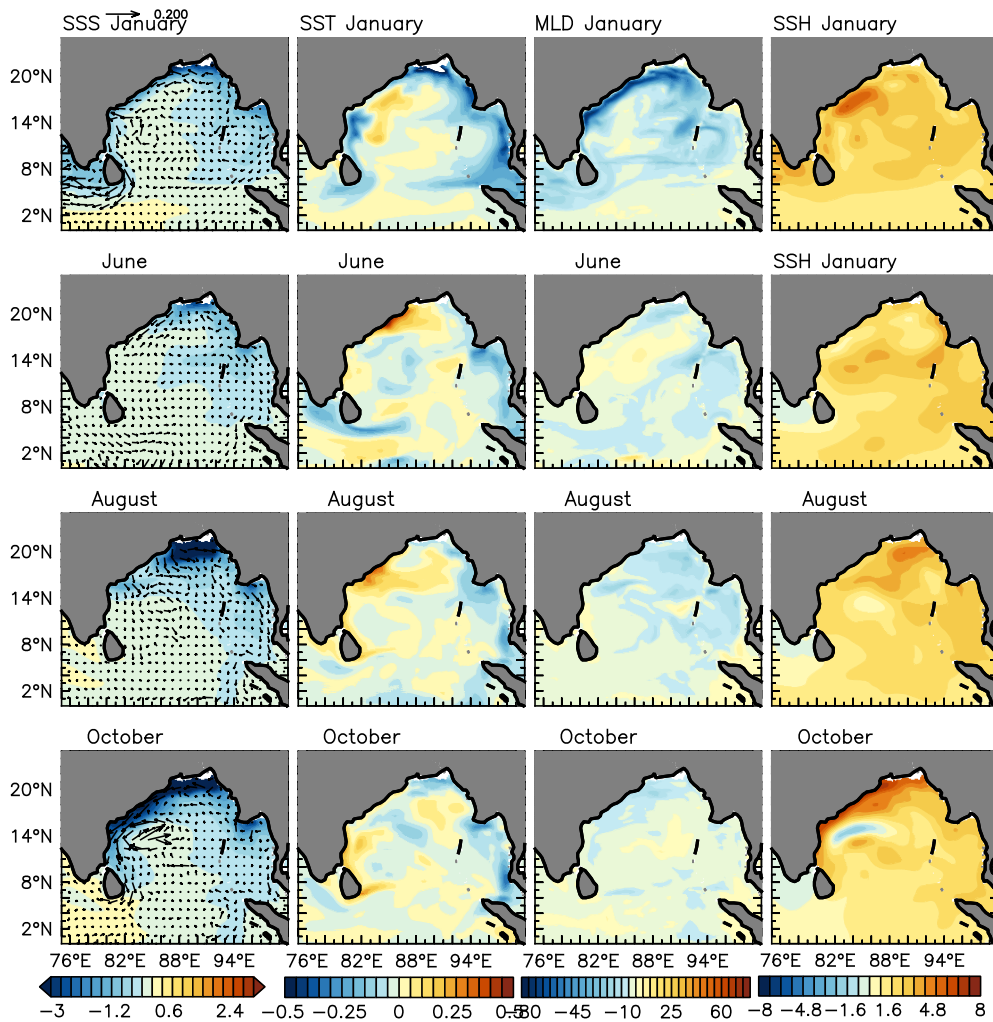


Figure 8: Difference between RIVER and NORIVER for SSS (psu, shaded, 1st column) and currents (m/s, vectors, 1st column), SST (°C, 2nd column), MLD (m, 3rd column) and SSH (cm, 4th column) for January (1st row), June (2nd row), August (3rd row), and October (4th row).

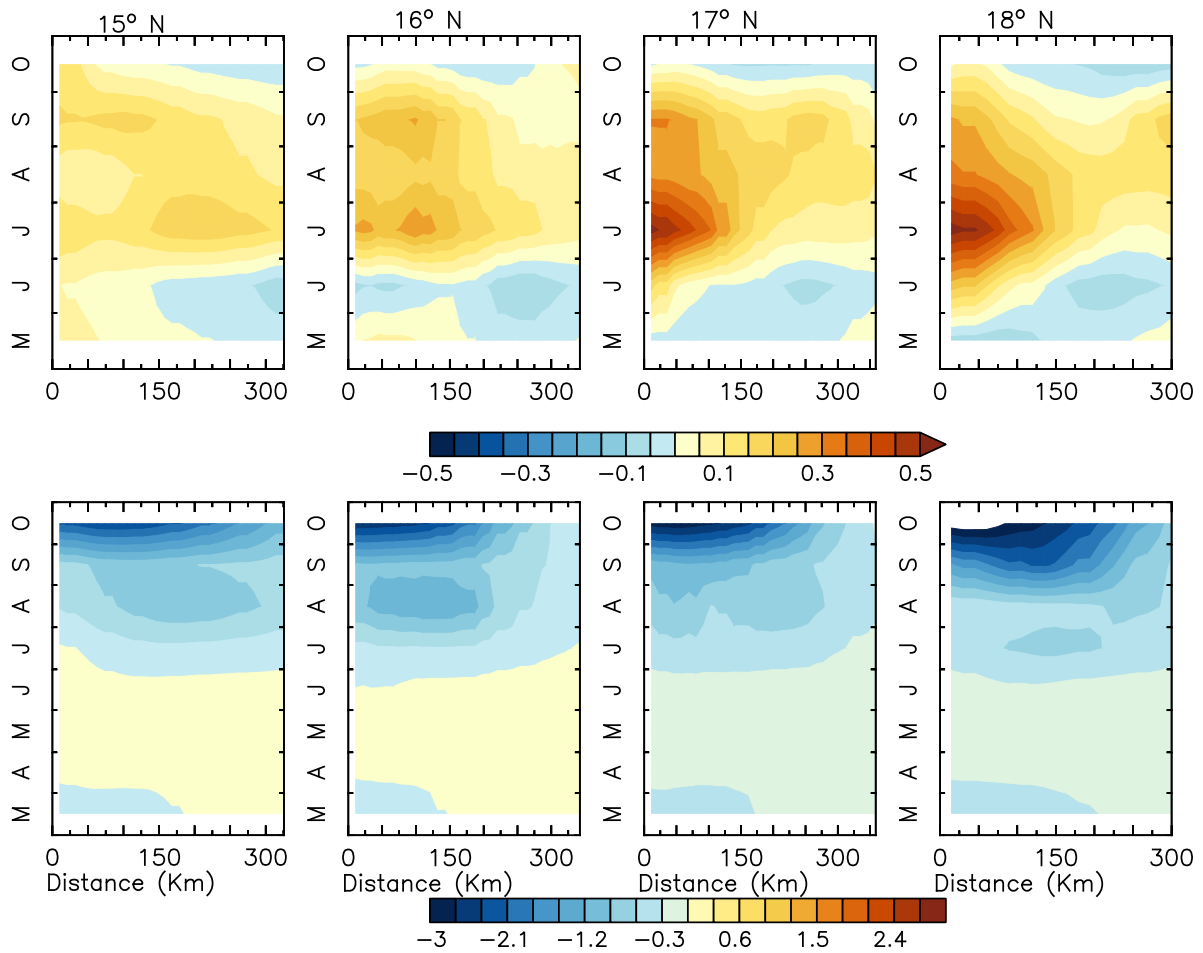


Figure 9: May to October cross-shore sections of the difference between RIVER and NORIVER for SST ($^{\circ}\text{C}$, 1st row) and Salinity (psu, 2nd row) for the sections marked at 18°N, 17°N, 16°N, 15°N in the right panel of Figure 3.

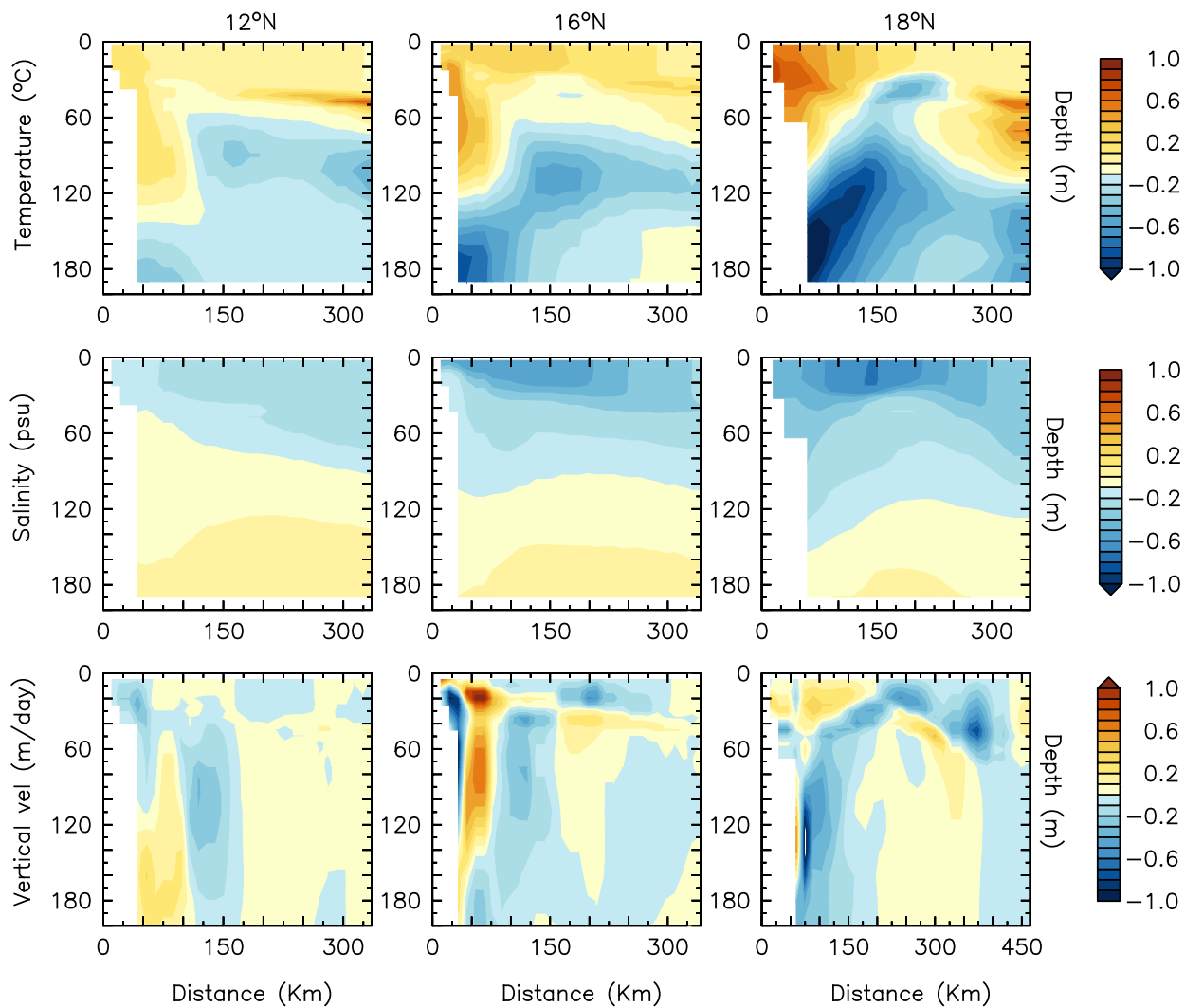


Figure 10: Vertical structure of the difference between RIVER and NORIVER for Temperature (1st row), Salinity (2nd row), and Vertical velocity (3rd row) for the month of July for the sections marked at 12°N, 16°N and 18°N in the right panel of Figure 3.

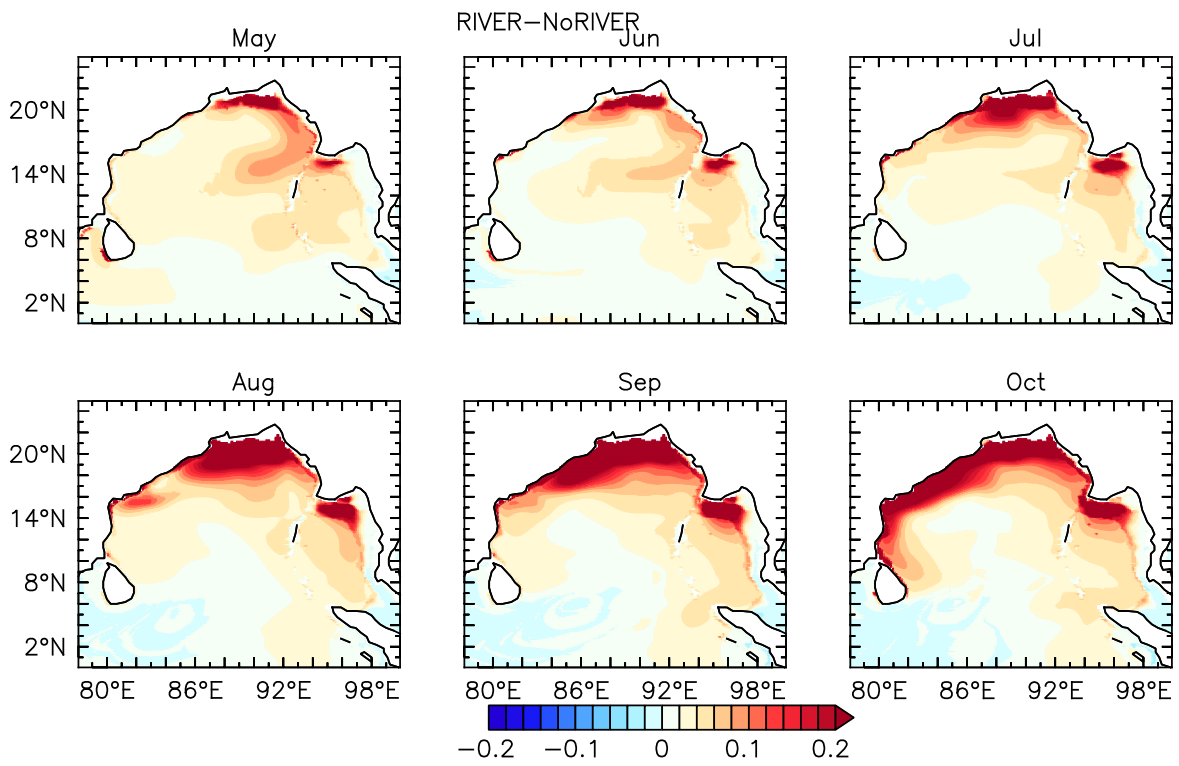


Figure 11: Difference in ocean salinity stratification (OSS, cph) between RIVER and NORIVER from May-October.

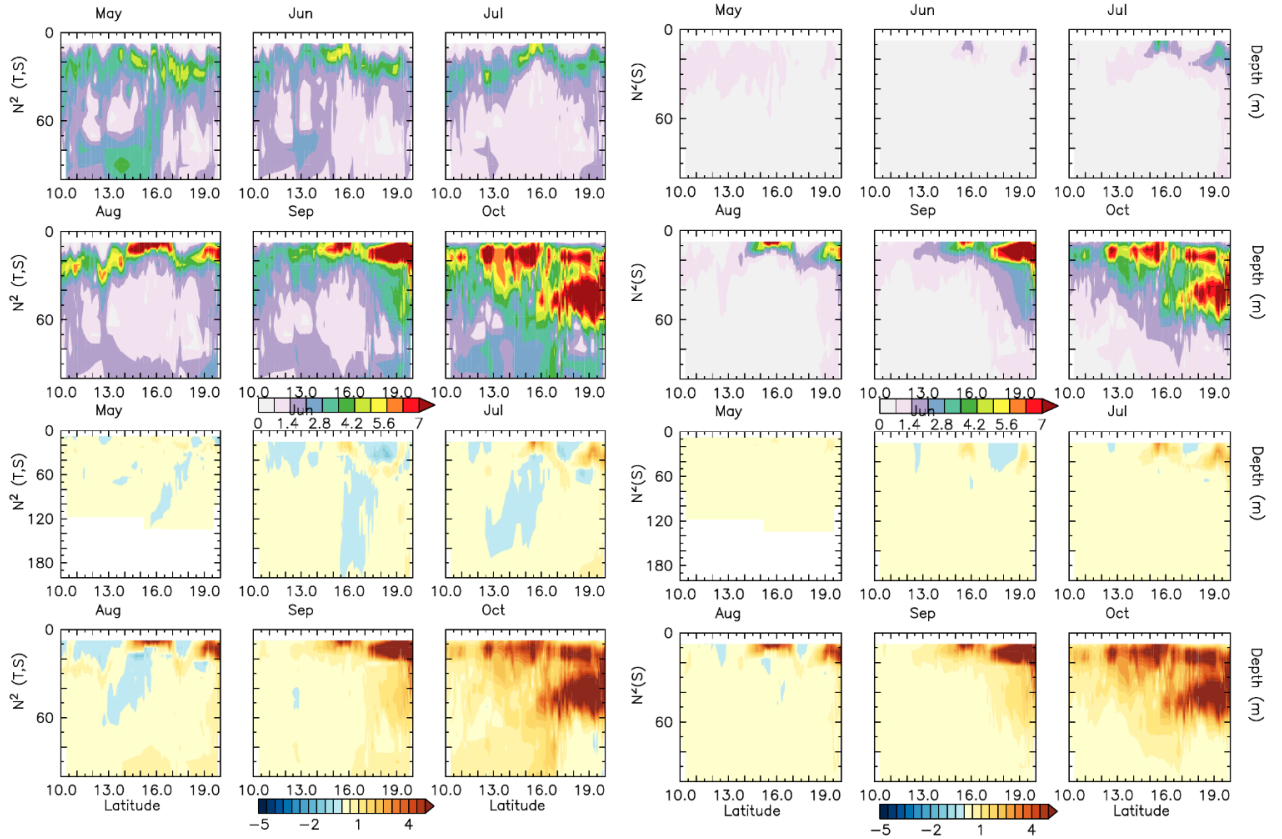


Figure 12: Left three columns. Vertical structure of N^2 (T,S) ($\times 10^{-4}$ /s), from the RIVER (first three columns, 1st and 2nd row) and the difference between RIVER and NORIVER (first three columns, 3rd and 4th row). Right three columns. N^2 (S) ($\times 10^{-4}$ /s), from the RIVER (last three columns, 1st and 2nd row) and the difference between RIVER and NORIVER (last three columns, 3rd and 4th row). All the plots are for data along the 100 m isobath shown in the right panel of Figure 3 from May-October.